Powder Technology 203 (2010) 57–69

Contents lists available at ScienceDirect

Powder Technology

journal homepage: www.elsevier.com/locate/powtec

Direct numerical simulation of gas–solid suspensions at moderate Reynolds number: Quantifying the coupling between hydrodynamic forces and particle velocity fluctuations

S. Tenneti [a], R. Garg [a], C.M. Hrenya [c], R.O. Fox [b], S. Subramaniam [a,*]

[a] Department of Mechanical Engineering, Center for Computational Thermal-fluids Research, Iowa State University, Ames, IA 50011, USA
[b] Department of Chemical and Biological Engineering, Iowa State University, Ames, IA 50011, USA
[c] Department of Chemical and Biological Engineering, University of Colorado, Boulder, CO 80309, USA

ARTICLE INFO

Available online 10 April 2010

Keywords:
Gas–solid suspension
Granular temperature
Particle acceleration model
Immersed boundary method
Particle-resolved direct numerical simulation

ABSTRACT

Predictive device-level computational fluid dynamics (CFD) simulation of gas–solid flow is dependent on accurate models for unclosed terms that appear in the averaged equations for mass, momentum and energy conservation. In the multifluid theory, the second moment of particle velocity represents the strength of particle velocity fluctuations and is known to play an important role in the prediction of core-annular flow structure in risers (Hrenya and Sinclair, AIChEJ, 43 (4) (1994) [5]). In homogeneous suspensions the evolution of the second velocity moment is governed by the particle acceleration–velocity covariance. Therefore, fluctuations in the hydrodynamic force experienced by particles in a gas–solid flow affect the evolution of particle velocity fluctuations, which in turn can affect the mean and variance of the hydrodynamic force. This coupling has been studied in the limit of Stokes flow by Koch and co-workers using a combination of kinetic theory and multipole expansion simulations. For Reynolds numbers beyond the Stokes limit, direct numerical simulation is a promising approach to quantify this coupling. Here we present direct numerical simulation (DNS) results for the evolution of particle granular temperature and particle acceleration variance in freely evolving homogeneous gas–solid suspensions. It is found that simple extension of a class of mean particle acceleration models to their corresponding instantaneous versions does not recover the correlation of particle acceleration with particle velocity. This study motivates the development of better instantaneous particle acceleration models that are able to accurately capture the coupling between particle acceleration and velocity.

1. Introduction

Gas–solid flows are commonly encountered in energy generation and chemical processing. The design and scale-up of industrial devices motivate a better understanding of gas–solid flow characteristics and transport phenomena. A fundamental understanding of gas–solid flow is increasingly relevant with renewed interest in zero-carbon and carbon-negative energy generation technology such as chemical looping combustion.

Computational fluid dynamics (CFD) simulations that solve for averaged equations of multiphase flow are being increasingly used in the design process because they provide detailed information about the solid volume fraction and phasic mean velocity fields in gas–solid flow [1]. Most CFD codes for device-level simulations of gas–solid flow are based on the Eulerian–Eulerian (EE) multifluid approach because these are computationally less expensive than Lagrangian–Eulerian (LE) simulations. In the EE multifluid approach both the solid and fluid phases are treated as interpenetrating continua, and averaging techniques [2–4] are used to derive the equations governing the conservation of average mass and momentum in the fluid and particle phases. This results in a closure problem similar to that encountered in the statistical theory of single-phase turbulence because the averaging procedure results in unclosed terms that need to be modeled. For instance, the mean momentum conservation equation in the particle phase requires closure of the average fluid–particle interaction force (mean drag force) and the average stress in the solid particle phase. Accurate models for these unclosed terms are needed for predictive CFD simulation of gas–solid flow.

As with all statistical closures, an important modeling question is the adequacy of the mathematical representation to capture physical phenomena of engineering relevance. For instance, it is now established that the prediction of core-annular structure in riser flows requires solving the transport equation for the particle granular temperature or pseudo-thermal energy [5]. This informs us that a closure at the level of mean quantities is not adequate to predict important flow characteristics such as core-annular structure, but a

* Corresponding author.
E-mail address: shankar@iastate.edu (S. Subramaniam).

0032-5910/$ – see front matter © 2010 Elsevier B.V. All rights reserved.
doi:10.1016/j.powtec.2010.03.042

closure at the level of second moments is necessary. However, it is not clear that closure at the level of the second moments is sufficient for predictive CFD simulation that will facilitate design and scale-up. Closure at the level of third-order moments has been attempted by some researchers [6,7].

An alternative approach to the closure of moment transport equations is to consider the evolution of the one-particle distribution function. Just as closure at the level of the transport equation for the probability density function (PDF) in single-phase turbulent reactive flow implies a closure for all moment equations, similarly a kinetic equation that achieves a closure for the one-particle distribution function in kinetic theory implies a closure for all moment equations. In particular, a closure at the one-particle distribution level automatically implies closure of the mean momentum and particle velocity second moment equations. Furthermore, closures at the one-particle distribution level are guaranteed to satisfy realizability criteria, whereas special care is needed to ensure the same in the case of moment closures. These considerations motivate the development of models for the unclosed terms in the transport equation for the one-particle distribution function corresponding to gas–solid flow.

While there is considerable work on kinetic theory of granular flows where the interaction with ambient fluid is neglected, the kinetic theory of gas–solid flow is still being developed. For low Reynolds number flow in the Stokes regime, Koch and co-workers [8,9] developed a kinetic theory closure with a model for the conditional particle acceleration that accounts for the presence of ambient fluid in the term transporting the distribution function in velocity space. This theoretical framework allows us to consider two coupled effects: (i) the effect of particle velocity fluctuations on the mean drag, and (ii) the effect of fluctuating particle acceleration on particle velocity fluctuations or granular temperature. Wylie et al. [10] studied the effect of particle velocity variance on the mean drag for the limiting case of high Stokes number where the particles move under elastic collisions but are unaffected by hydrodynamic forces. They showed that particle velocity fluctuations do not affect the mean drag in Stokes flow. This result is not surprising because in Stokes flow the particle acceleration is a linear function of instantaneous particle velocity. However, at moderate mean slip Reynolds numbers the drag law is nonlinear and Wylie et al. [10] showed that particle velocity fluctuations do affect the mean particle acceleration. They proposed a modified drag law in terms of volume fraction ϕ, mean flow Reynolds number Re_m and Reynolds number based on particle granular temperature Re_T. The focus of this paper is on the second effect: the effect of fluctuating hydrodynamic forces on granular temperature.

For statistically homogeneous gas–solid flows, the correlation between the particle fluctuating velocity and its acceleration fluctuation determines the evolution of the particle velocity second moment. In the limiting case of Stokes flow, Koch [8,9] analyzed the granular temperature, which is the trace of the particle velocity second moment, and decomposed the particle acceleration–velocity covariance as the sum of source and sink contributions. Particle granular temperature decreases due to inelastic collisions and viscous interactions with the ambient fluid, and these effects are represented by the sink term. If particle collisions are elastic or flow past fixed particle assemblies is considered, then the granular temperature decreases only due to viscous interactions with the ambient fluid. In the Stokes flow regime the sink term simply relaxes the granular temperature to zero on the viscous relaxation time scale. In Koch's decomposition of the acceleration–velocity covariance into source and sink terms [9], the source term due to hydrodynamic interactions with neighboring particles can balance the sink term leading to a steady state granular temperature in stable homogeneous suspensions. For moderate Reynolds number, there is no unique decomposition of the particle acceleration–velocity covariance as the sum of source and sink contributions.

The source term in the granular temperature equation plays an important role in sustaining a nonzero value of the granular temperature. In its absence the granular temperature in a homogeneous suspension would simply decay to zero, leading to an infinite Mach number in the particle phase. Not only is this problematic from a numerical standpoint for CFD simulations, but it is also unphysical over a wide range of mean flow Reynolds number and volume fraction. The origin of the source term lies in the hydrodynamic interactions that each particle experiences with its neighbors, and the range of this interaction depends on the mean flow Reynolds number and the solid volume fraction. It is well known that a sphere sedimenting in a fluid can have a “drafting” effect on its neighbors and draw them into its wake. The draft, kiss and tumble phenomena are well documented in [11]. These physical mechanisms can manifest as a source in particle velocity fluctuations by changing each particle's velocity. This effect is quantified through DNS of freely evolving suspensions in this work.

Although Koch's analysis is useful in the Stokes flow regime, it is difficult to extend the analysis to moderate Reynolds number cases. At moderate Reynolds number, DNS offers a promising approach to quantify unclosed terms in the transport equations for particle velocity moments, or the transport equation for the one-particle distribution function. This naturally leads to an evaluation of existing models. We use DNS of gas–solid flow at moderate Reynolds number to evaluate a class of acceleration models. The results indicate the need for improved instantaneous particle acceleration models that are capable of capturing the coupling between particle velocity fluctuations and hydrodynamic forces in gas–solid flow.

The next section describes pertinent details of the statistical modeling approach that motivate this study. This is followed by a description of the Particle-resolved Uncontaminated-fluid Reconcilable Immersed Boundary Method (PUReIBM) that is used to perform DNS of gas–solid flow. Then the simulation details for fixed particle assemblies and freely moving suspensions are presented. Results that quantify the coupling are reported, and a class of particle acceleration models is evaluated. Finally, the conclusions of this study are summarized.

2. Statistical models

The averaged equations for mean momentum conservation and transport of the second moment of particle velocity in the multifluid theory can be derived using either the Eulerian–Eulerian or Lagrangian–Eulerian approach. A comprehensive summary of the relations between the moment equations obtained from these statistical approaches can be found in [12]. Here we choose the Lagrangian–Eulerian approach with the one-particle distribution function as our starting point because it naturally leads to an explicit connection with the moment equations.

2.1. One-particle distribution function

The one-particle distribution function, which is the number density of particles in an appropriately defined phase space, is the fundamental quantity of interest in the kinetic theory of granular and multiphase flow [8,14–17]. It is also referred to as the droplet distribution function in spray theory [18]. For monodisperse particles the distribution function $f(\mathbf{x}, \mathbf{v}, t)$ is defined in a position–velocity space, and evolves by the following transport equation:

$$\frac{\partial f}{\partial t} + \nabla_{\mathbf{x}}\cdot(\mathbf{v}f) + \nabla_{\mathbf{v}}\cdot(\langle \mathbf{A}|\mathbf{x},\mathbf{v};t\rangle f) = \dot{f}_{\text{coll}}, \tag{1}$$

where $\nabla_{\mathbf{x}}$ and $\nabla_{\mathbf{v}}$ denote the gradient operators in the position and velocity space, respectively, and $\dot{f}_{\text{coll}}$ is the collisional term that can depend on higher-order statistics. A closure model for the collisional term results in a kinetic equation. This well-known equation has been extensively studied in the context of granular flows where collisions

are inelastic. Extensions to non-dilute cases that follow the Enskog approach have also been pursued. The focus in the kinetic theory of granular flow is on obtaining closed-form solutions [19], or constitutive relations [17,20–23], starting from a kinetic equation. Most of these studies rely on the Chapman–Enskog expansion about a normal solution in terms of a nonuniformity parameter that is essentially the Knudsen number.

The principal difference between the kinetic theory of gases and the kinetic theory of gas–solid flow is that in the latter, the conditional particle acceleration term $\langle \mathbf{A}|\mathbf{x},\mathbf{v};t\rangle$ appears inside the velocity derivative in the velocity transport term because particle drag depends on particle velocity through slip with respect to the fluid. This dependence of particle acceleration on particle velocity in Eq. (1) results in the correlation of $\mathbf{A}$ and $\mathbf{v}$ that determines the evolution of the second moment of particle velocity, and its trace, the particle granular temperature. In the transport equation for the distribution function (cf. Eq. (1)), $\langle \mathbf{A}|\mathbf{x},\mathbf{v};t\rangle$ represents the average particle acceleration conditional on position $\mathbf{x}$ and velocity $\mathbf{v}$. For the spatially homogeneous case with monodisperse particles it can be interpreted as the average acceleration experienced by a particle with velocity $\mathbf{v}$. The averaging operator $\langle\cdot\rangle$ represents integration over all higher-order multiparticle distribution functions [8,15] that can be defined on the basis of the ensemble of particles with position and velocity $\{\mathbf{X}^{(n)}(t), \mathbf{V}^{(n)}(t), n=1, \ldots, N\}$. In particular, the conditional acceleration $\langle \mathbf{A}|\mathbf{x},\mathbf{v};t\rangle$ is obtained by integrating out its dependence on the two-particle density (pair correlation function). In other words, the conditional acceleration $\langle \mathbf{A}|\mathbf{x},\mathbf{v};t\rangle$ is not completely determined by the particle velocity, but may be affected by the presence of neighbor particles. The statistical description of multiparticle interactions is not contained in the one-particle distribution function.

Subramaniam [16] notes that when the gas phase is represented by Reynolds-averaged fields, a class of models for the unclosed conditional acceleration term $\mathbf{A}^*$ can be written as:

$$\langle \mathbf{A}|\mathbf{x},\mathbf{v};t\rangle = \mathbf{A}^*\left(\left\{\langle Q_g(\mathbf{x},t)\rangle\right\}, q(f(\mathbf{x},\mathbf{v},t)), \mathbf{x},\mathbf{v},\ldots;t\right), \tag{2}$$

where $\{\langle Q_g(\mathbf{x}, t)\rangle\}$ represents a set of averaged fields from the gas-phase solution (such as the mean gas velocity and turbulent kinetic energy), and $q(f)$ is any simply computed function of the distribution function. The ellipsis denotes the dependence on statistical quantities that are not represented in the distribution function, e.g., dependence on higher-order multiparticle statistics, or fluid-phase statistics not represented in $\{\langle Q_g(\mathbf{x}, t)\rangle\}$. Recall that the physical origins of the source term in the granular temperature equation lie in the hydrodynamic interactions with neighbor particles and fluid-phase velocity fluctuations. The statistics of neighbor particles are not contained in $f(\mathbf{x}, \mathbf{v}, t)$. If the implementation of the multifluid theory accounts for fluid-phase velocity fluctuations, then this dependence can be incorporated in the acceleration model of Eq. (2). However, many implementations of the multifluid theory do not account for fluid-phase velocity fluctuations.

As noted earlier, closure of the transport equation for the distribution function (cf. Eq. (1)) implies closure for all moment equations. In the following, the implied closure for the mean and second moment of particle velocity is examined.

2.2. Moment equations

The averaged equations for mean momentum conservation and transport of the second moment of particle velocity implied by Eq. (1) are derived using the usual procedure to derive hydrodynamic equations in kinetic theory, except for the fact that the velocity dependence in the conditional acceleration results in an additional term in the second moment equation [8,12]. Here these equations are discussed in the context of modeling the conditional acceleration $\langle \mathbf{A}|\mathbf{x},\mathbf{v};t\rangle$ to capture the coupling between particle velocity fluctuations and hydrodynamic force. Since the DNS results we present in this study are for fixed particles or for those undergoing elastic collisions, the moment equations are presented for the case of elastic collisions only.

2.2.1. Mean particle velocity

The mean momentum conservation equation written in index notation is

$$\frac{\partial}{\partial t}\left(\rho_p\phi\langle v_j\rangle\right) + \frac{\partial}{\partial x_k}\left(\rho_p\phi\langle v_j\rangle\langle v_k\rangle\right) = \rho_p\phi\langle A_j\rangle - \frac{\partial}{\partial x_k}\left(\rho_p\phi\langle v_j'' v_k''\rangle\right), \tag{3}$$

where ρ_p is the particle density, ϕ is the solid volume fraction given by $\phi = n\pi d_p^3/6$, where n is the number density of the particles and d_p is the particle diameter. For gas–solid flow, the mean particle acceleration $\langle \mathbf{A}\rangle$ due to the fluid–particle drag force is an unclosed term in Eq. (3). In EE multifluid theory, the mean particle acceleration $\langle \mathbf{A}\rangle$ is modeled using a drag law as

$$\langle \mathbf{A}\rangle = -\beta\langle \mathbf{W}\rangle, \tag{4}$$

where $\langle \mathbf{W}\rangle = \langle \mathbf{v}\rangle - \langle \mathbf{u}^{(f)}\rangle$ is the mean slip velocity between the solid and fluid phases. In this definition, $\langle \mathbf{u}^{(f)}\rangle$ and $\langle \mathbf{v}\rangle$ are the fluid and solid phase-averaged velocities, respectively. For an isolated particle in Stokes flow, β is a constant equal to $3\pi\mu_f d_p$, where μ_f is the dynamic viscosity of the fluid. The Reynolds number based on the mean slip velocity between the fluid and particulate phase quantifies the relative importance of fluid inertia, and is defined as

$$\mathrm{Re}_m = (1-\phi)\frac{\rho_f\left|\langle \mathbf{v}\rangle - \left\langle \mathbf{u}^{(f)}\right\rangle\right| d_p}{\mu_f}, \tag{5}$$

where ρ_f is the density of the fluid. When the Reynolds number based on the mean slip Re_m is moderate ($\mathrm{Re}_m > 1$), β is a function of the mean slip velocity between the particle and the fluid phase, i.e. $\beta = \beta(|\langle \mathbf{W}\rangle|)$, and the drag is no longer linearly dependent on the mean slip velocity.

Typical drag laws for gas–solid flow [24–26] characterize the dependence of fluid–particle drag force on the mean slip Reynolds number and solid volume fraction. These are obtained by a combination of fitting experimental data and using semi-analytical approaches in limiting cases. More recently, direct numerical simulation of flow past homogeneous fixed particle assemblies has been used to deduce drag laws ([27–29]) describing the dependence on mean slip Reynolds number and solid volume fraction.

In the mean particle velocity evolution equation, the last term on the right hand side of Eq. (3) is the transport of particle Reynolds stress arising from correlation of particle velocity fluctuations. Particle velocity fluctuations are defined about the mean velocity as

$$\mathbf{v}'' = \langle \mathbf{v} - \mathbf{v}\rangle, \tag{6}$$

and the particle granular temperature[1] that characterizes the strength of these fluctuations is

$$T = \frac{1}{3}\langle \mathbf{v}''\cdot\mathbf{v}''\rangle. \tag{7}$$

This term is calculated by solving a transport equation for the particle velocity covariance.

[1] Note that we do not distinguish between particle velocity fluctuations arising from collisions and other sources, as suggested by Breault et al. [13]. Our definition is consistent with the standard definition in kinetic theory of granular and gas–solid flow, and it is also the definition adopted in the two-fluid theory.

2.2.2. Transport of particle velocity covariance

The evolution equation for the second moment of velocity written in index notation is [8,9,12]

$$\frac{\partial}{\partial t}\left(\rho_p\phi\langle v_i'' v_j''\rangle\right) + \frac{\partial}{\partial x_k}\left(\rho_p\phi\langle v_i'' v_j''\rangle\langle v_k\rangle\right) = -\frac{\partial}{\partial x_k}\left(\rho_p\phi\langle v_i'' v_j'' v_k''\rangle\right) - \rho_p\phi\left(\langle v_i'' v_k''\rangle\frac{\partial\langle v_j\rangle}{\partial x_k} + \langle v_j'' v_k''\rangle\frac{\partial\langle v_i\rangle}{\partial x_k}\right) + \rho_p\phi\left(\langle A_i'' v_j''\rangle + \langle A_j'' v_i''\rangle\right). \tag{8}$$

For statistically homogeneous gas–solid flow with no mean velocity gradients the transport, production, and triple-velocity correlation terms drop out and Eq. (8) reduces to

$$\frac{\partial}{\partial t}\left(\rho_p\phi\langle v_i'' v_j''\rangle\right) = \rho_p\phi\left(\langle A_i'' v_j''\rangle + \langle A_j'' v_i''\rangle\right), \tag{9}$$

showing that the particle velocity covariance evolves according to the particle acceleration–velocity covariance (fluctuations in the acceleration are defined about the mean acceleration, i.e. $A''_j = A_j - \langle A_j\rangle$.) This equation shows how fluctuations in the hydrodynamic forces affect the particle velocity covariance. Contracting the indices in Eq. (9) results in the evolution of particle granular temperature for a statistically homogeneous gas–solid flow:

$$\frac{dT}{dt} = \frac{2}{3}\langle A_i'' v_i''\rangle. \tag{10}$$

In the above equation, the trace of the particle acceleration–velocity covariance $\langle A''_i v''_i\rangle$ can be either a positive or negative quantity, and hence it can act as a source or a sink of granular temperature.

2.2.3. Mean and fluctuating particle acceleration

From this discussion of moment equations we see that the mean acceleration affects mean momentum, and fluctuations in acceleration correlate with fluctuating velocity to act as a source or sink term in the granular temperature equation. In the following, we relate the mean acceleration and acceleration fluctuations to the one-particle distribution function.

The mean acceleration $\langle\mathbf{A}\rangle$ is obtained as the integral of the conditional expectation of particle acceleration over velocity space:

$$\langle\mathbf{A}\rangle(\mathbf{x},t) = \frac{1}{n(\mathbf{x},t)}\int_{[\mathbf{v}]}\langle\mathbf{A}\,|\,\mathbf{x},\mathbf{v};t\rangle f(\mathbf{x},\mathbf{v},t)d\mathbf{v}, \tag{11}$$

and this leads to the expression $\langle\mathbf{F}^{fp}\rangle = \rho_p - \phi\langle\mathbf{A}\rangle$ for the fluid–particle drag (per unit volume) in the mean particle momentum equation. The expression for the mean acceleration is useful because it tells us how the velocity dependence in the conditional acceleration can affect the mean drag through the distribution function. The one-particle distribution function can be decomposed [16] into the product of a number density $n(\mathbf{x}, t)$ and a velocity probability density function $f^c_{\mathbf{V}}(\mathbf{v};\mathbf{x},t)$:

$$f(\mathbf{x},\mathbf{v},t) = n(\mathbf{x},t)f^c_{\mathbf{V}}(\mathbf{v};\mathbf{x},t). \tag{12}$$

Therefore, changes in the distribution and level of particle velocity fluctuations are characterized by the particle velocity probability density function $f^c_{\mathbf{V}}(\mathbf{v};\mathbf{x},t)$, and these affect the mean drag through Eq. (11).

In the kinetic theory description of gas–solid flow using the one-particle distribution function, the fluctuating acceleration is simply the difference between the conditional and unconditional mean: $\mathbf{A}'' = \langle\mathbf{A}|\mathbf{v}\rangle - \langle\mathbf{A}\rangle$. Using this definition, the particle acceleration–velocity covariance can be written in terms of the one-particle distribution function as

$$\langle A_i'' v_j''\rangle = \frac{1}{n}\int_{[\mathbf{v}]}\{\langle A_i\,|\,\mathbf{v}\rangle - \langle A_i\rangle\}v_j'' f(\mathbf{v},t)d\mathbf{v}. \tag{13}$$

As noted earlier, fluctuations in particle acceleration can arise from particle velocity fluctuations, hydrodynamic interactions with neighbor particles, and fluid-phase velocity fluctuations. While Eq. (13) explicitly accounts for the effect of particle velocity fluctuations, the other effects must be incorporated in the model for the conditional particle acceleration.

2.2.4. Modeling the conditional particle acceleration

A straightforward extension of the mean particle acceleration model given by Eq. (4) to its conditional counterpart is

$$\mathbf{A}^* = -\beta\mathbf{W} = -\beta\left(\mathbf{v} - \langle\mathbf{u}^{(f)}\rangle\right), \tag{14}$$

where $\mathbf{A}^*$ represents a model (cf. Eq. (2)) for the conditional particle acceleration $\langle\mathbf{A}|\mathbf{v}\rangle$, and $\mathbf{W}$ is the instantaneous slip velocity. Here we have written the instantaneous slip velocity as the difference between the instantaneous particle velocity and the mean fluid velocity, rather than as the difference between the instantaneous velocities in each phase, i.e. $\mathbf{W} = \mathbf{v} - \mathbf{u}$. This is because in CFD models based on the multifluid theory there is no representation of the instantaneous gas-phase velocity and the gas-phase motions are represented only by the mean gas velocity. Although this simple model results in the same mean drag as in Eq. (4), its implied closure for the acceleration–velocity covariance in the granular temperature equation results in only a sink of granular temperature. This is because the simple extension in Eq. (14) does not represent the effects of neighboring particles or fluctuations in the fluid velocity relative to its mean.

For Stokes flow, Koch [8] derived an analytical closure for the source term in the granular temperature equation (cf. Eq. (10)) using a kinetic equation applicable to a dilute monodisperse gas–solid suspension with high particle inertia. He defined the instantaneous slip velocity as $\mathbf{W} = \mathbf{v} - \mathbf{u}^{(i)}$, where $\mathbf{u}^{(i)}$ is the fluid velocity excluding the direct effect of the ith particle (but including the disturbance effects of all the other particles). This definition of the slip velocity gives rise to a source term in the granular temperature equation. Linearity of the governing equations in the Stokes flow limit and the assumption of a dilute suspension allowed the derivation of an explicit expression for $\mathbf{u}^{(i)}$ and the source term. For moderately dense suspensions, the assumptions made by Koch [8] in the kinetic theory approach are not valid and hence Koch and Sangani [9] used a semi-analytical approach that used multipole expansion simulations to derive an expression for the source of granular temperature in the Stokes flow limit.

In Section 2.3, we review the closures for the source term given by [8] and [9] in the Stokes flow limit. Developing similar closures for $\langle\mathbf{A}|\mathbf{x},\mathbf{v};t\rangle$ and the source term at moderate Reynolds numbers is difficult because the governing Navier–Stokes equations are nonlinear. In Section 3, we present a direct numerical simulation methodology based on PUReIBM as a promising approach to develop closures for the source and sink terms in the granular temperature equation at moderate Reynolds numbers.

2.3. Closure for high Stokes number particles undergoing elastic collisions in Stokes flow

In a high Stokes number suspension the particle velocities are not significantly affected by hydrodynamic forces. For a dilute suspension of very massive particles (high Stokes number) undergoing perfectly elastic collisions in Stokes flow, Koch [8] showed that the steady state particle velocity distribution in the kinetic theory description is Maxwellian.[2] Therefore, in this limit the particle velocity covariance

[2] Later Koch and Sangani [9] used an approximate multipole method to show that even for dense suspensions of elastic particles in Stokes flow, the velocity distribution is Maxwellian.

tensor is isotropic and its evolution can be simply described by the granular temperature evolution equation.

2.3.1. Dilute suspensions of perfectly elastic particles

For a dilute homogeneous suspension of highly massive and perfectly elastic monodisperse particles in Stokes flow, the evolution equation of the granular temperature derived by Koch [8] is

$$\frac{dT}{dt} = -\frac{2R}{\tau}T + \frac{2S_I}{3}. \tag{15}$$

The first term on the right hand side of Eq. (15) is the sink of particle granular temperature due to viscous dissipation. In this term, $R = 1 + 3\phi^{1/2}/\sqrt{2}$ is the dimensionless particle momentum relaxation rate and $\tau = m/(6\pi\mu_f a)$ is the characteristic time scale over which the velocity of a particle of mass m and radius a relaxes due to viscous forces. The second term on the right hand side of Eq. (15) is the source due to hydrodynamic interactions. In the dilute limit, the expression for this source term is

$$S_I = \left(apt\left|\langle \mathbf{W}\rangle\right|^2\right) / \left(2\pi^{1/2}\tau^2 T^{1/2}\right). \tag{16}$$

The source term in the dilute limit is denoted S_I to distinguish it from the source term S_{II} at higher volume fractions that are discussed in the following section.

2.3.2. Moderately dense to dense suspensions of perfectly elastic particles

Koch and Sangani [9] used the multipole expansion method to evaluate the source term due to hydrodynamic forces for dense homogeneous suspensions of massive elastic particles in Stokes flow. In their simulation the particles move as a granular gas and their motion is not affected by the interstitial fluid. The evolution equation for the granular temperature is written as

$$\frac{dT}{dt} = -\frac{2R_{\mathrm{diss}(\phi)}}{\tau}T + \frac{2S_{II}}{3}. \tag{17}$$

For the sink term due to viscous dissipation (first term on the right hand side of Eq. (17)), the expression for the dimensionless dissipation rate $R_{\mathrm{diss}(\phi)}$ as a function of volume fraction given by [30] is used. The source term in granular temperature (second term on the right hand side of Eq. (17)) is expressed as an integral of the temporal autocorrelation of the force experienced by the particles. The final expression for the source term given by [9] is

$$S_{II} = \frac{a}{\tau^2}\frac{\left|\langle \mathbf{W}\rangle\right|^2}{T^{1/2}}S^*(\phi) \tag{18}$$

where $S^*(\phi)$ is the dimensionless source term. Expressions for the dimensionless dissipation rate and the dimensionless source as a function of the volume fraction can be found in [9].

3. Direct numerical simulation approach

Here we describe a DNS approach based on the Particle-resolved Uncontaminated-fluid Reconcilable Immersed Boundary Method (PUReIBM) that is used to solve for flow past arbitrary arrangements of solid spherical particles. Two types of simulation results are presented: (i) for fixed particle assemblies, and (ii) for freely moving suspensions. The hydrodynamic solver that is common to both types of simulations is first described. Then the solution approach for fixed particle assemblies is outlined. This is followed by a description of the simulations of freely evolving suspensions where the positions and velocities of the particles evolve under the action of hydrodynamic and collisional forces.

3.1. Hydrodynamic solver

PUReIBM is a particle-resolved direct numerical simulation approach for gas–solid flow where the continuum Navier–Stokes equations with no-slip and no-penetration boundary conditions on each particle's surface are solved using a forcing term that is added to the momentum equation. The salient features that distinguish PUReIBM from other immersed boundary method approaches are as follows:

1. Uncontaminated fluid: In PUReIBM the immersed boundary (IB) forcing is solely restricted to those grid points that lie in the solid phase, and therefore the flow solution in the fluid phase is uncontaminated by the IB forcing. Consequently the velocity and pressure in the fluid phase is a solution to the unmodified Navier–Stokes equations (in contrast to IB implementations that smear the IB forcing on to grid points in the fluid phase adjoining solid boundaries, resulting in solution fields that do not correspond to unmodified Navier–Stokes equations).
2. Reconcilable: In PUReIBM the hydrodynamic force experienced by a particle is computed directly from the stress tensor at the particle surface that is obtained from this uncontaminated-fluid flow solution (in contrast to IB implementations that calculate the hydrodynamic force from the IB forcing field). This feature of PUReIBM enables us to directly compare the DNS solution with any random-field theory of multiphase flow. In particular, for statistically homogeneous suspensions it is shown by Garg et al. [29] that if the volume-averaged hydrodynamic force exerted on the particles by the fluid is computed from a PUReIBM simulation, it is a consistent numerical calculation of the average interphase momentum transfer term $\langle \tau'_{ji} n_j^{(s)} \delta(\mathbf{x} - \mathbf{x}^{(l)})\rangle$ in the two-fluid theory [3]. This reconciles DNS results with multiphase flow theory.

Owing to these specific advantages, it is shown elsewhere [29,31] that PUReIBM is a numerically convergent and accurate particle-resolved DNS method for gas–solids flow. Its performance has been validated in a comprehensive suite of tests: (i) Stokes flow past simple cubic (SC) and face centered cubic (FCC) arrangements (ranging from dilute to close-packed limit) with the boundary-integral method of [32], (ii) Stokes flow past random arrays of monodisperse spheres with LBM simulations of [33] (iii) moderate to high Reynolds numbers ($\mathrm{Re_m} \leq 300$) in SC and FCC arrangements with LBM simulations of [34] and (iv) high Reynolds number flow past random arrays of monodisperse spheres with ANSYS-FLUENT CFD package. It has also been extended to study passive scalar transport, and validated for heat transfer from a single isolated sphere [31].

The numerical scheme used in PUReIBM is a primitive-variable, pseudo-spectral method, using a Crank–Nicolson scheme for the viscous terms, and an Adams–Bashforth scheme for the convective terms. A fractional time-stepping method that is based on Kim and Moin's approach [35] is used to advance the velocity fields in time. The principal advantage of the PUReIBM approach is that it enables the use of regular Cartesian grids to solve for flow past arbitrarily shaped moving bodies without the need for costly remeshing. It also considerably simplifies parallelization of the flow solver as compared to unstructured body-fitted grids.

3.2. Fixed particle assemblies

The particle configuration for DNS of flow past fixed assemblies is generated by first allowing particles to attain a random spatial arrangement through elastic collisions. A homogeneous configuration of non-overlapping spheres corresponding to the specified solid volume fraction is generated with particle centers on a lattice, and particles are assigned a Maxwellian velocity distribution. Particles are allowed to equilibrate under purely elastic collisions (in the absence of any interstitial fluid) to generate a homogeneous particle configuration for the DNS flow solver. Ensemble-averaged flow

statistics are obtained by averaging over multiple independent simulations (MIS) performed with several such configurations. Each statistically identical configuration corresponds to the same average solid volume fraction and pair correlation (macrostate), but differs in the specific arrangement of particles (microstates). The PUReIBM simulation methodology and details of the computation of the mean acceleration (or mean drag) for a fixed particle assembly are described by Garg et al. [29].

3.3. Freely evolving suspensions

Numerical simulations [36] of freely evolving suspensions have been performed to study the sedimentation of monodisperse particles under gravity in the presence of a fluid. Simulations of freely sedimenting suspensions are carried out in periodic domains such that the imposed pressure gradient in the fluid balances the weight of the particles. In sedimentation calculations the steady mean flow Reynolds number attains a unique value that depends on the problem parameters (fluid and particle densities, solid volume fraction and the value of acceleration due to gravity), and this value is not known *a priori*. In the present study we seek to simulate freely evolving particle suspensions at arbitrary mean slip Reynolds numbers while maintaining the solid/fluid density ratio and solid volume fraction at fixed values. We also want to specify the mean flow Reynolds number as input to the simulation. This can be accomplished by specifying a mean pressure gradient that does not exactly balance the weight of the particles, but exerts the requisite body force to maintain the desired slip velocity between the particles and fluid. However, now both the mean particle velocity and the mean fluid velocity change in time because there is no steady solution in the laboratory frame to the mean momentum balance in each phase. Note that even though the mean phasic velocities are evolving in time, their difference—the mean slip velocity—attains a steady value.

The difficulty in simulating this flow setup in the laboratory frame with periodic boundary conditions is that the continuous increase in fluid and particle velocities places unnecessary restrictions on the time step through the Courant condition. To circumvent this problem we developed a different simulation setup that performs the DNS in an accelerating reference frame such that the particles have a zero mean velocity with respect to the computational grid. The equations of motion are solved in an accelerating frame of reference that moves with the mean velocity of the particles. In this frame, the particles execute only fluctuating motion. In our setup, particles *on average* do not flow in or out of the computational domain, thereby maintaining a reasonable time step that is based on the mean slip velocity. Particles do flow in and out of the domain because of their fluctuating velocity. The advantage of our setup is that the desired mean flow Reynolds number is specified as an input parameter, and we are able to solve the problem with reasonable time steps that resolve the flow. Details of the equations solved in the accelerating reference frame are given in Appendix A.

In the freely evolving DNS, each particle moves with an acceleration that arises from hydrodynamic and collisional forces. The particles are represented in a Lagrangian frame of reference at time t by $\{\mathbf{X}^{(i)}(t), \mathbf{V}^{(i)}(t)\ i=1, \ldots, N_p\}$, where $\mathbf{X}^{(i)}(t)$ denotes the ith particle's position and $\mathbf{V}^{(i)}(t)$ denotes its translational velocity. The position and translational velocity of the ith particle evolve according to Newton's laws as:

$$\frac{d\mathbf{X}^{(i)}(t)}{dt} = \mathbf{V}^{(i)}(t), \tag{19}$$

$$m\frac{d\mathbf{V}^{(i)}}{dt} = \mathbf{B} + \mathbf{F}_d^{(i)}(t) + \sum_{\substack{j=1 \\ j\neq i}}^{N_p} \mathbf{F}_{ij}^{c}(t), \tag{20}$$

where $\mathbf{B}$ is any external body force (zero in the simulations shown here), $\mathbf{F}_d^{(i)}$ is the hydrodynamic force (from pressure and viscous stress that is calculated from the velocity and pressure fields at the particle surface) and $\mathbf{F}_{ij}^{c}$ is the contact force on the ith particle as a result of collision with jth particle. Particle–particle interactions are treated using soft-sphere collisions based on a spring-dashpot contact mechanics model that was originally proposed by Cundall and Strack [37]. The advantage of using soft-sphere collisions is that the simulations can be extended to higher volume fractions because enduring multiparticle contacts are taken into account. In the soft-sphere approach, the contact mechanics between two overlapping particles is modeled by a system of springs and dashpots in both normal and tangential directions. The spring causes colliding particles to rebound, and the dashpot mimics the dissipation of kinetic energy due to inelastic collisions. The spring stiffness coefficients in the tangential and normal directions are k_t and k_n, respectively. Similarly, the dashpot damping coefficients in the tangential and normal directions are η_t and η_n, respectively. The spring stiffness and dashpot damping coefficients are related to the coefficient of restitution and the coefficient of friction (see [38] for details of the implementation).

The particles considered in this study are assumed to be perfectly elastic and frictionless. Since the particles are perfectly elastic, the damping force arising from the dashpot is zero. The tangential component of the contact force is zero for frictionless particles. Therefore, only the normal component of the spring force $\mathbf{F}_{nij}^{S}$ contributes to the contact force $\mathbf{F}_{ij}^{c}$ at time t:

$$\mathbf{F}_{ij}^{c}(t) = \mathbf{F}_{nij}^{S}(t). \tag{21}$$

At the initiation of contact, the normal spring force $\mathbf{F}_{nij}^{S}$ is equal to $-k_n\delta_{ij}$, where δ_{ij} is the overlap between the particles computed using the relation

$$\delta_{ij} = d_p - \left|\mathbf{X}^{(i)} - \mathbf{X}^{(j)}\right|. \tag{22}$$

A time history of the spring forces is maintained once the contact initiates. At any time during the contact, the normal spring force is given by

$$\mathbf{F}_{nij}^{S}(t+\Delta t) = \mathbf{F}_{nij}^{S}(t) - k_n\mathbf{V}_{nij}\Delta t, \tag{23}$$

where $\mathbf{V}_{nij}$ is the relative velocity in the normal direction (defined below) that is computed using

$$\mathbf{V}_{nij} = \left[\left(\mathbf{V}^{(i)} - \mathbf{V}^{(j)}\right)\cdot\hat{\mathbf{r}}_{ij}\right]\hat{\mathbf{r}}_{ij}. \tag{24}$$

The normal vector $\hat{\mathbf{r}}_{ij}$ is the unit vector along the line of contact pointing from particle i to particle j. The governing equations of motion that are solved in the fluid, and the details of the computation of the hydrodynamic force acting on the particles are discussed in Appendix A.

A homogeneous particle configuration is generated in the same way as for the fixed particle assemblies by equilibrating an ensemble of particles undergoing elastic collisions in the absence of interstitial fluid. Following the simulation methodology of [29], a steady flow at the desired mean flow Reynolds number is first established for this fixed particle assembly. Once the mean fluid–particle drag experienced by this fixed particle assembly reaches a steady state, the particles are released at time $t=0$ for the freely evolving DNS simulation.

The particles are advanced on a time step Δt_{coll} that is determined by the spring stiffness and the dashpot coefficients. The flow fields are updated on a time step Δt_{fluid}, which ensures that both the convective and viscous time scales are well resolved. At the start of a flow time step the forces acting on the particles are computed based on the flow fields obtained at the end of the previous flow time step. If Δt_{coll} is

smaller than Δt_{fluid} the particles are stepped by Δt_{coll} until the end of the flow time step, otherwise both the particles and the fluid are stepped by Δt_{coll}. The simulation is continued until the granular temperature reaches a steady state.

4. Results

We first present results from a validation test for fixed particle assemblies. We then quantify particle acceleration and its coupling to fluctuations in the particle velocity in flow past fixed particle assemblies as well as freely moving suspensions.

4.1. Fixed particle assemblies

Simulations with fixed particle positions and velocities are representative of physical fluid-particle systems in which the particle velocities do not change significantly over characteristic fluid time scales (the relevant scale here being the time to transit a characteristic length scale such as the particle diameter at the mean slip velocity). This is true for high Stokes number (gas–solid) suspensions. Simulations of flow past fixed particle assemblies are less computationally demanding than freely evolving suspensions, and are useful for parametric studies (variation of mean flow Reynolds number and mean solid volume fraction). This approach has been extensively used to deduce computational drag laws for homogeneous gas–solid (high Stokes number) suspensions by many researchers [27,28,33,34,39]. Here we use this test to compare PUReIBM DNS results with existing LBM-based drag correlations.

The mean drag obtained from PUReIBM DNS is compared with the LBM-based drag correlation of [34] in Fig. 1. The normalized mean fluid–particle force F is defined as

$$F = \frac{|\langle \mathbf{f} \rangle|}{3\pi\mu_f d_p |\langle \mathbf{W} \rangle|} \tag{25}$$

where $\langle \mathbf{f} \rangle$ is the average fluid–particle force per particle. The PUReIBM DNS results show an excellent match with the drag correlation of [34].

The validation test shown here is performed with all the particles at rest, so the fluctuations in particle velocity are zero. If a random velocity is assigned to each particle in the fixed bed according to a Maxwellian distribution corresponding to a specified value of the particle granular temperature, then the fixed bed simulation can be considered an instantaneous snapshot of a freely evolving suspension. Of course in a freely evolving suspension the dynamic response of the particles to the hydrodynamic forces will affect the particle velocity fluctuations, and this is not captured by the fixed bed simulation. Nevertheless, this still allows us to consider the effect of particle velocity fluctuations on the hydrodynamic forces, albeit in a limited sense.

The magnitude of particle velocity fluctuations is characterized by defining a Reynolds number based on the granular temperature Re_T as:

$$\text{Re}_T = \frac{\rho_f d_p T^{1/2}}{\mu_f}. \tag{26}$$

In Fig. 2 we plot the streamwise component of fluctuating acceleration A'_x for each particle versus its fluctuation in the streamwise velocity component v'_x for $\text{Re}_m = 20$ and $\text{Re}_T = 16$ at a solid volume fraction of 0.2. The first observation is that A'_x and v'_x are negatively correlated. This is to be expected because as seen from the schematic of the flow setup in Fig. 3, a positive fluctuation in particle velocity results in a lower slip velocity that corresponds to a lower drag value because of the relation $\mathbf{A} \propto -\mathbf{W}$ for isolated particles. This manifests as a negative fluctuation in particle acceleration. However, the second interesting observation from the scatter plot in Fig. 2 is that some positive fluctuations in velocity actually result in positive fluctuations in the acceleration. In other words, the presence of neighbor particles and the resulting hydrodynamic interactions can occasionally violate the $\mathbf{A} \propto -\mathbf{W}$ relation for isolated particles. Also the fluid velocity in the proximity of the particle can be significantly different from the mean fluid velocity, and the definition of the instantaneous slip as $\mathbf{W} = \mathbf{v} - \langle \mathbf{u}^{(f)} \rangle$ may not accurately represent the instantaneous slip velocity. The joint statistics of particle acceleration and particle velocity represent the coupling between hydrodynamic forces and particle velocity fluctuations. In particular, the acceleration–velocity covariance is important for accurate prediction of the particle granular temperature evolution.

We now investigate the predictions for joint particle acceleration–velocity statistics using a simple model (this model is used in other works such as [10] to predict the effect of particle velocity fluctuations

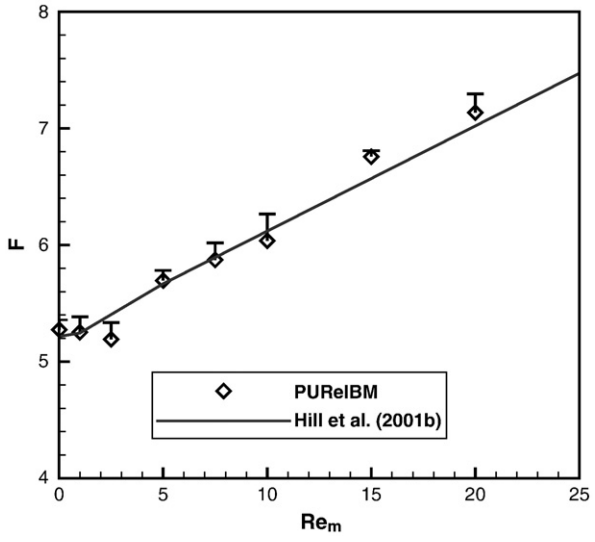

Fig. 1. The comparison of the mean drag obtained from PUReIBM simulations with the drag correlation reported by [34] at a solid volume fraction of 0.2 for the baseline case of zero particle velocity fluctuations.

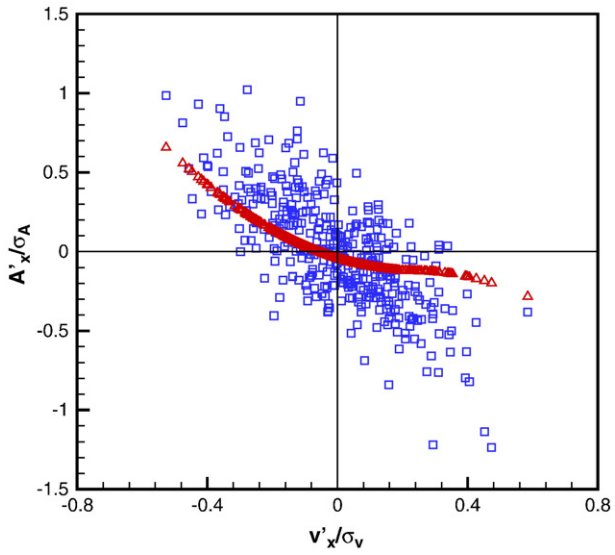

Fig. 2. Scatter plot of streamwise component of fluctuating acceleration versus the streamwise component of fluctuating velocity. Square symbols (□) show fluctuations in the particle acceleration obtained from DNS using PUReIBM simulations, while upper triangles (△) show fluctuations in the particle acceleration predicted by simple extension of a mean drag law to its instantaneous counterpart.

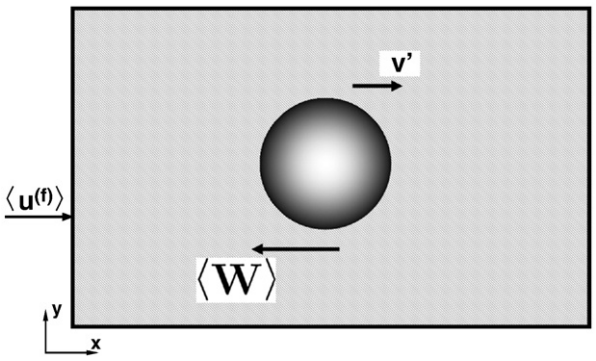

Fig. 3. Schematic of the flow setup. The mean velocity of the fluid phase $\langle \mathbf{u}^{(f)} \rangle$ is directed along the positive x axis as shown. The mean velocity $\langle \mathbf{v} \rangle$ of the particles is zero and so the mean slip velocity $\langle \mathbf{W} \rangle = \langle \mathbf{v} \rangle - \langle \mathbf{u}^{(f)} \rangle$ is along the negative x axis. The solid particle shown in this figure has a positive velocity fluctuation $\mathbf{v}'$ along the positive x axis. The schematic illustrates that a positive fluctuation about the mean velocity of the particles implies a reduced instantaneous slip velocity, $\mathbf{v}' - \langle \mathbf{u}^{(f)} \rangle$ between the particle and the fluid.

on mean drag). The instantaneous counterpart of the acceleration model described in Eq. (14),

$$\mathbf{A} = -\beta \mathbf{W},$$

is used to compute the instantaneous particle acceleration for each particle velocity value in the DNS. In this model β is taken from the drag correlation proposed by Hill et al. [34]. The acceleration–velocity scatter plot obtained from this model is also shown in Fig. 2 (upper triangles). One can see that this simple extension of the mean acceleration model does not recover the scatter obtained in the DNS, but instead it predicts a significantly different joint statistical behavior. The data points in quadrants Q1 and Q3 that are found in the scatter plot from DNS are totally absent in the model. Clearly this comparison points to the need for an improved model for the conditional particle acceleration in the velocity transport term in the evolution equation for the one-particle distribution function in the kinetic theory of multiphase flow.

While useful information regarding instantaneous particle acceleration–velocity joint statistics can be extracted from fixed particle simulations, they are inadequate to characterize the temporal evolution of the particle granular temperature. For this purpose we perform DNS of freely evolving suspensions.

4.2. Freely moving suspensions

DNS of a freely evolving suspension in periodic domain is performed for a volume fraction of $\phi = 0.2$. Unlike sedimentation studies where the mean slip velocity is limited by the settling velocity of the particles in suspension, here we solve the equations of motion in an accelerating frame of reference so that arbitrary mean flow Reynolds numbers $\mathrm{Re_m}$ can be simulated. A value of $\mathrm{Re_m} = 20$ is chosen for the simulations reported here, which is well outside the Stokes regime. Three different particle to fluid density ratios ($\rho_p/\rho_f = 10$, 100 and 1000) are used to analyze the dynamics of the system.

First we examine the mean fluid–particle drag in the freely evolving suspension for different values of the particle to fluid density ratio. The time evolution of the normalized drag F (cf. Eq. (25)) is shown in Fig. 4(a). Fig. 4(a) shows that the mean drag in the suspension for a particle to fluid density ratio of 1000 varies slowly in time when compared to the other two cases. This is because the particle configuration changes very slowly due to high inertia of the particles. Thus, when compared to the other two density ratios, the behavior of this system is expected to be much closer to that of a fixed

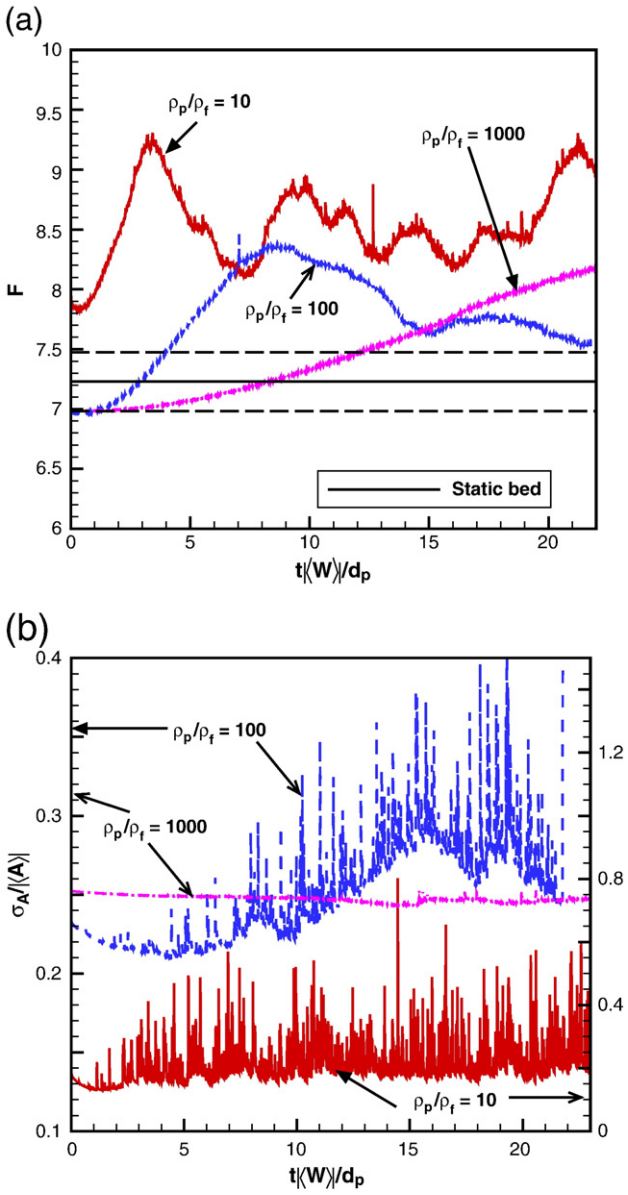

Fig. 4. (a) Shows the evolution of the normalized mean drag at a volume fraction of 0.2 and a mean flow Reynolds number of 20 for three different particle to fluid density ratios: $\rho_p/\rho_f = 10$ (red), 100 (blue), and 1000 (purple). The black solid line indicates the drag in a static bed at the same mean flow Reynolds number and volume fraction. The dashed lines represent 95% confidence limits on the mean drag for the static bed. (b) Shows the evolution of the standard deviation of fluctuations in the particle acceleration relative to the mean drag at a volume fraction of 0.2 and a mean flow Reynolds number of 20 for different density ratios. In this plot, data for $\rho_p/\rho_f = 10$ are shown on the right hand side y-axis. The standard deviation in the acceleration obtained for a fixed bed is 0.22.

bed. However, even the case with density ratio of 1000 is not identical to a fixed bed with zero particle velocity fluctuations because of the changing particle configuration, nonzero particle velocity fluctuations and the effect of added mass in the hydrodynamic force. Nevertheless, it is clear that as the density ratio increases the mean drag experienced by the particles in a freely evolving suspension is better approximated by the corresponding fixed bed simulation.

The fluctuations in the particle acceleration play a very important role in the dynamics of the suspension as discussed earlier. In Fig. 4 (b), the level of acceleration fluctuations σ_A relative to the mean acceleration is plotted with time for the three density ratios. It can be seen that the particle acceleration fluctuations are almost constant for

the suspension with the highest density ratio of 1000. The steady value of $\sigma_A/|\langle \mathbf{A}\rangle|$ for the case with highest density ratio is very close to that obtained from a fixed assembly of particles at the same volume fraction of 0.2 and mean flow Reynolds number of 20.

The plot of acceleration fluctuations in Fig. 4(b) has several significant implications. First of all, it tells us that the steady state value of $\sigma_A/|\langle \mathbf{A}\rangle|$ in freely evolving suspensions is not negligible. Therefore, fluctuating hydrodynamic forces (relative to the mean drag) are important not just in the Stokes regime, but at moderate Reynolds numbers also. Secondly, it informs us that the level of acceleration fluctuations in freely evolving suspensions is not very different from that in fixed particle assemblies. This partially justifies the calculation of joint acceleration–velocity statistics from fixed particle assemblies and their comparison with a simple model that was presented earlier. The third inference we draw from Fig. 4(b) is that the instantaneous particle acceleration model must represent the increasing level of temporal variations in fluctuating hydrodynamic force that accompany a decrease in particle to fluid density ratio.

We now quantify the effect of the fluctuations in the hydrodynamic force on particle velocity fluctuations in freely evolving suspensions. The evolution of granular temperature for the three different particle to fluid density ratio values that are considered is shown in Fig. 5. Details of the estimation of granular temperature from DNS of freely evolving suspensions are given in Appendix B.

As expected, the lower density ratio cases attain a higher steady granular temperature, and the rate at which the steady value is reached is inversely proportional to the particle to fluid density ratio. The value of the scaled granular temperature is relatively low when compared with the turbulence intensity in single-phase turbulence. It indicates a high Mach number in the particle phase (on the order of 100 for a scaled granular temperature of 10^{-4}). This indicates that the particles in the gas–solid suspension are not dominated by collisions like molecular gases at STP, but rather they are closer to a supercooled state. For comparison, the values of granular temperature in Stokes flow as estimated by the theory of Koch and Sangani [9] are 2 to 3 orders of magnitude smaller than the DNS results shown here for a mean flow Reynolds number of 20.

5. Conclusions

The coupling between hydrodynamic forces and particle velocity fluctuations in gas–solid suspensions at moderate Reynolds number is studied using direct numerical simulation of freely evolving suspensions that imposes no-slip and no-penetration boundary conditions on the surface of each particle. The DNS results show that fluctuations in particle acceleration are significant at moderate Reynolds numbers. The standard deviation in acceleration relative to the mean acceleration ranges from 0.2 to 0.4 depending on the particle to fluid density ratio. This extends current understanding of this coupling that has been extensively studied by Koch and co-workers in the limit of Stokes flow. Another key finding that emerges from this work is that the steady state granular temperature from DNS of freely evolving suspensions at $Re_m = 20$ is two to three orders of magnitude larger than that predicted by the theory of Koch and Sangani [9] for Stokes flow. A simple extension of drag laws for mean particle acceleration (based on the mean slip velocity) to model the instantaneous particle acceleration does not recover the correct acceleration–velocity covariance that is obtained from DNS. This work motivates the development of better models for instantaneous particle acceleration that are capable of accurately representing the coupling between hydrodynamic forces and particle velocity fluctuations.

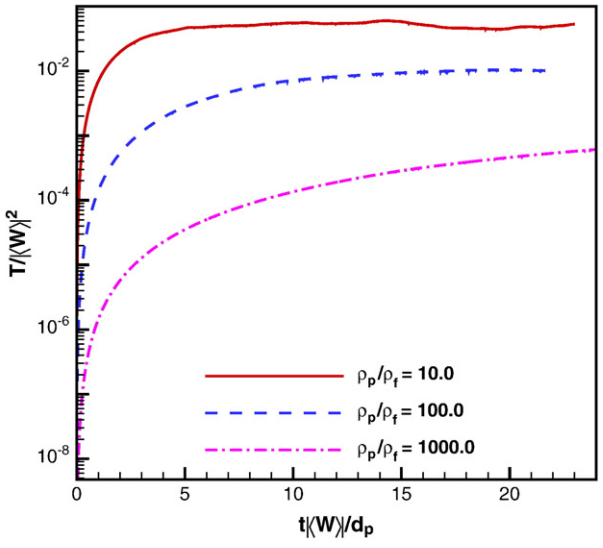

Fig. 5. Evolution of the particle granular temperature at a volume fraction of 0.2 and a mean flow Reynolds number of 20 for different density ratios.

Nomenclature

f	one-particle distribution function (s^3/m^6)
$\dot{f}_{coll}$	source of the one-particle distribution function due to particle collisions (s^2/m^6)
$\mathbf{v}$	sample space variable for velocity of the particle (m/s)
$\mathbf{x}$	position vector (m)
x, y, z	components of the position vector $\mathbf{x}$ (m)
v_x, v_y, v_z	components of the velocity vector $\mathbf{v}$ (m/s)
$\nabla_{\mathbf{x}}$	gradient operator in position space given by $\mathbf{i}\frac{\partial}{\partial x} + \mathbf{j}\frac{\partial}{\partial y} + \mathbf{k}\frac{\partial}{\partial z}$
$\nabla_{\mathbf{v}}$	gradient operator in velocity space given by $\mathbf{i}\frac{\partial}{\partial v_x} + \mathbf{j}\frac{\partial}{\partial v_y} + \mathbf{k}\frac{\partial}{\partial v_z}$
t	time (s)
$\mathbf{i}, \mathbf{j}, \mathbf{k}$	unit vectors in the x, y and z directions respectively
$\langle \mathbf{A}\|\mathbf{x}, \mathbf{v}; t\rangle$	Conditional expectation of particle acceleration (m/s^2)
$p(\mathbf{x}, t)$	fluid pressure field (N/m^2)
$\langle \mathbf{A}\rangle$	unconditional expectation of particle acceleration (m/s^2)
$\langle \mathbf{f}\rangle$	average fluid–particle force per particle (N)
$\langle \mathbf{v}\rangle$	average particle velocity (m/s)
$\langle \mathbf{F}^{fp}\rangle$	mean fluid–particle drag (N)
$\langle \bar{\mathbf{g}}\rangle_\nu$	mean pressure gradient in the accelerating frame (N/m^3)
$\langle \mathbf{u}^{(f)}\rangle$	phasic averaged fluid velocity (m/s)
$\langle \mathbf{u}^{(s)}\rangle$	phasic averaged solid velocity (m/s)
$\langle \mathbf{W}\rangle$	mean slip velocity between the solid and the fluid phases (m/s)
β	interphase momentum transfer coefficient (s^{-1})
$\bar{\mathbf{x}}$	position vector in the accelerating frame (m)
$\mathbf{B}$	external body force (N)
$\mathbf{W}$	instantaneous particle slip velocity (m/s)
$\mathbf{V}^{(i)}$	velocity vector of the ith particle (m/s)
$\mathbf{X}^{(i)}$	position vector of the ith particle (m)
$\{T\}$	granular temperature estimated from DNS (m^2/s^2)
$\{\mathbf{u}^{(s)}\}$	mean solids velocity estimated from DNS (m/s)
$\Delta\bar{t}$	time step in the accelerating frame (s)
Δt_{coll}	time step used to resolve particle–particle collisions (s)
Δt_{fluid}	time step used to resolve flow field (s)
δ_{ij}	overlap between the particles i and j (m)
$\langle \bar{\mathbf{g}}\rangle_\nu^{n+1}$	mean pressure gradient at $(n+1)$th time step in the accelerating frame (N/m^3)
$\langle \bar{\mathbf{u}}^{(f)}\rangle^d$	desired mean fluid velocity in the accelerating frame (m/s)
$\langle \bar{\mathbf{u}}^{(f)}\rangle^{n+1}$	mean fluid velocity at $(n+1)$th time step in the accelerating frame (m/s)
$\langle \bar{\mathbf{u}}^{(s)}\rangle^{n+1}$	mean solid velocity at $(n+1)$th time step in the accelerating frame (m/s)
$\langle \bar{\mathbf{u}}^{(f)}\rangle^{n}$	mean fluid velocity at nth time step in the accelerating frame (m/s)
$\langle \bar{\mathbf{u}}^{(s)}\rangle^{n}$	mean solid velocity at nth time step in the accelerating frame (m/s)
$\bar{\mathbf{F}}_D^n$	total drag force acting on the solid particles at nth time step

in the accelerating frame (N)
$\mathbf{A}_{\mathrm{f}}^{n+1}$ frame acceleration at $(n+1)$th time step (m/s^2)
η_{n} dashpot damping coefficient in the normal direction used in the soft-sphere collision model (N s/m)
η_{t} dashpot damping coefficient in the tangential direction used in the soft-sphere collision model (N s/m)
$\mathbf{F}^{\mathrm{S}}_{\mathrm{n}ij}$ normal component of the spring force between particles i and j that arises in the soft-sphere collision model (N)
$\mathbf{F}_{\mathrm{d}}^{(i)}$ total drag force acting on the ith particle (N)
$\hat{\mathbf{r}}_{ij}$ unit vector along the line of contact pointing from particle i to particle j
$\mathcal{V}_{\mathrm{s}}^{(n)}$ region occupied by the nth particle
$\mathbf{F}^{\mathrm{c}}_{ij}$ contact force on the ith particle due to collision with jth particle (N)
$\mathcal{V}$ region of the physical domain
$\mathcal{V}_{\mathrm{f}}$ region occupied by the fluid phase
$\mathcal{V}_{\mathrm{s}}$ region occupied by the solid phase
Re_{T} Reynolds number based on the particle granular temperature
μ_{f} dynamic viscosity of the fluid (N s/m^{-2})
ν_{f} kinematic viscosity of the fluid (m^2/s)
$\bar{\mathbf{F}}_{\mathrm{D}}$ total drag force acting on the solid particles (N)
$\bar{\mathbf{g}}$ pressure gradient in the accelerating frame (N/m^3)
$\bar{\mathbf{g}}'$ fluctuating pressure gradient in the accelerating frame (N/m^3)
$\bar{\mathbf{S}}$ convective term of the Navier–Stokes equations in the accelerating frame (m/s2)
$\bar{t}$ time in the accelerating frame (s)
$\partial\mathcal{V}$ boundary of the periodic box
$\partial\mathcal{V}_{\mathrm{s}}$ interface between the solid and the fluid phases
$\partial\mathcal{V}_{\mathrm{s}}^{(n)}$ surface of the nth particle
ϕ solid volume fraction
Re_{m} Reynolds number based on the mean slip velocity
ρ_{f} thermodynamic density of the fluid (kg/m^3)
ρ_{p} thermodynamic density of the particles (kg/m^3)
σ_{A} standard deviation in the particle accelerations (m/s^2)
τ viscous relaxation time scale (s)
$\mathbf{V}_{\mathrm{n}ij}$ relative velocity between the particles i and j in the normal direction (m/s)
d_{p} particle diameter (m)
dA infinitesimal area element on the surface of the sphere (m^2)
F normalized mean fluid–particle force per particle
$f^{\mathrm{c}}_{\mathbf{v}}$ velocity probability density function (s^3/m^3)
k_{n} spring stiffness coefficient in the normal direction used in the soft-sphere collision model (N/m)
k_{t} spring stiffness coefficient in the tangential direction used in the soft-sphere collision model (N/m)
m mass of the particle (kg)
n number density (1/m^3)
N_{p} number of particles in the domain
R dimensionless particle momentum relaxation rate used by [8]
R_{diss} dimensionless dissipation rate used by [30]
S^* dimensionless source of granular temperature used by [8] and [30]
S_I source of granular energy in the dilute volume fraction limit derived by [8] (m^2/s^3)
S_{II} source of granular temperature in the moderate volume fraction limit given by [30] (m^2/s^3)
T particle granular temperature (m^2/s^2)
V volume of the physical domain (m^3)
V_{f} volume of the region occupied by fluid (m^3)
V_{s} volume of the region occupied by the solid phase (m^3)
$\bar{\mathbf{u}}(\bar{\mathrm{x}}, \bar{t})$ fluid velocity field in the accelerating frame (m/s)
$\mathbf{A}''$ particle acceleration fluctuations (m/s^2)
$\mathbf{A}^*$ modeled instantaneous particle acceleration (m/s^2)
$\mathbf{A}_{\mathrm{f}}$ frame acceleration (m/s^2)
$\mathbf{n}^{(n)}$ unit normal vector pointing outward from the surface of the nth particle
$\mathbf{n}^{(\mathrm{s})}$ Unit normal vector pointing outward from the surface of the solid
$\mathbf{u}(\mathbf{x}, t)$ fluid velocity field in the laboratory frame (m/s)
$\mathbf{u}^{(i)}$ fluid velocity excluding the direct effect of the ith particle used by [8] (m/s)
$\mathbf{v}''$ particle velocity fluctuations (m/s)
$\mathbf{v}'^{(n)}$ fluctuating velocity of the nth particle (m/s)
$\mathbf{V}_{\mathrm{f}}$ frame velocity (m/s)
ψ' fluctuating pressure (N/m^2)

Acronyms

CFD computational fluid dynamics
DNS direct numerical simulation
EE Eulerian–Eulerian
IB immersed boundary
IBM immersed boundary method
LE Lagrangian–Eulerian
MIS multiple independent simulations
PDF probability density function
PUReIBM Particle-resolved Uncontaminated-fluid Reconcilable Immersed Boundary Method

Acknowledgment

This work was supported by a Department of Energy grant DE-FC26-07NT43098 through the National Energy Technology Laboratory.

Appendix A. Equations of motion in an accelerating frame of reference

Consider a two-phase flow in a finite flow volume $\mathcal{V}$ in physical space as an ensemble of spherical particles as shown in Fig. 6. At time t, the nth particle is characterized by its position vector $\mathbf{X}^{(n)}(t)$ and its velocity vector $\mathbf{V}^{(n)}(t)$. A Lagrangian description is used for the particles and an Eulerian description is used for describing the motion of the fluid.

Denoting the velocity and pressure fields of the fluid by $\mathbf{u}(\mathbf{x}, t), p(\boldsymbol{x}, t)$ respectively, the governing equations of motion for the fluid phase in a reference frame E fixed in space (laboratory frame) are:

$$\frac{\partial u_i}{\partial x_i} = 0, \tag{A.1}$$

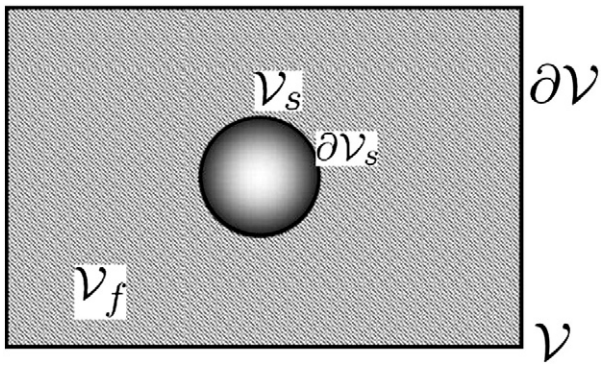

Fig. 6. Schematic of the physical domain. Hatched lines represent the volume $\mathcal{V}_{\mathrm{f}}$ occupied by the fluid phase, solid fill represents the volume $\mathcal{V}_{\mathrm{s}}$ occupied by the solid particle, and $\mathcal{V} = \mathcal{V}_f \cup \mathcal{V}_s$ is the total volume. $\partial\mathcal{V}$ and $\partial\mathcal{V}_{\mathrm{s}}$ represent, respectively, the areas of the computational box and the solid particle.

$$\frac{\partial u_i}{\partial t} + u_j \frac{\partial u_i}{\partial x_j} = -\frac{1}{\rho_f}\frac{\partial p}{\partial x_i} + \nu_f \frac{\partial^2 u_i}{\partial x_j \partial x_j}. \tag{A.2}$$

In the above equation, ρ_f, ν_f are the density and kinematic viscosity of the fluid respectively. These equations are to be solved with the boundary conditions $\mathbf{u}=\mathbf{V}^{(n)}(t)$ on $\partial\mathcal{V}_s^{(n)}(t)$. Here, $\partial\mathcal{V}_s^{(n)}(t)$ is the surface of the nth particle whose spatial location changes with time because of the motion of the particle. The governing equations of motion for the particles in the laboratory frame are:

$$m\frac{dV_i^{(n)}}{dt} = -\int_{\partial v_s^{(n)}(t)} p n_i^{(n)} dA + \mu_f \int_{\partial v_s^{(n)}(t)} \frac{\partial u_i}{\partial x_j} n_j^{(n)} dA \tag{A.3}$$

where $\mu_f=\rho_f\nu_f$ is the dynamic viscosity of the fluid. In the above equation, $n_j^{(n)}$ denotes the component of the normal pointing outward from the surface of the nth particle.

The objective here is to solve the equations of motion of both the phases in a reference frame that moves with the mean velocity of the particles. Since the particles will be accelerating in the laboratory frame, the new reference frame denoted $\overline{E}$ will be a non-inertial frame of reference. Let the velocity and acceleration of $\overline{E}$ with respect to the laboratory frame E be $\mathbf{V}_f(t)$ and $\mathbf{A}_f(t)$ respectively. The transformation rules between the two frames are:

$$\begin{aligned} \overline{\mathbf{u}} &= \mathrm{u} - \mathbf{V}_f, \\ \overline{\mathbf{x}} &= \mathbf{x} - \int_0^t \mathbf{V}_f(t')dt' \\ \overline{t} &= t. \end{aligned} \tag{A.4}$$

Effecting the transformation rules defined above into Eq. (A.2) the governing equations of motion for the fluid phase in E are (see [40] for details of the derivation)

$$\frac{\partial \overline{u}_i}{\partial \overline{x}_i} = 0, \tag{A.5}$$

$$\frac{\partial \overline{u}_i}{\partial \overline{t}} + \overline{u}_j \frac{\partial \overline{u}_i}{\partial \overline{x}_j} = -\frac{1}{\rho_f}\frac{\partial p}{\partial \overline{x}_i} + \nu_f \frac{\partial^2 \overline{u}_i}{\partial \overline{x}_j \partial \overline{x}_j} - A_{f,i}. \tag{A.6}$$

It should be noted that the pressure being a scalar remains the same in both the frames. Following the notation of [29], the momentum equation in Eq. (A.6) can be rewritten as

$$\frac{\partial \overline{u}_i}{\partial \overline{t}} + \overline{S}_i = -\frac{1}{\rho_f}\overline{g}_i + \nu_f \frac{\partial^2 \overline{u}_i}{\partial \overline{x}_j \partial \overline{x}_j} - A_{f,i} \tag{A.7}$$

where $\bar{\mathbf{S}}$ and $\bar{\mathbf{g}}$ respectively are the convective and pressure gradient terms in $\bar{E}$. It is assumed that the particle assemblies are homogeneous at all times. If the particle configuration is homogeneous then the ensemble averaged quantities can be estimated by volume averaging. The flow quantities can be decomposed as a sum of the volumetric mean and a fluctuating part. For instance, the pressure gradient can be decomposed as $\bar{\mathbf{g}}=\langle\bar{\mathbf{g}}\rangle_{\mathcal{V}}+\bar{\mathbf{g}}'$ where, the volumetric mean pressure gradient $\langle\bar{\mathbf{g}}\rangle_{\mathcal{V}}$ is defined as

$$\langle \overline{\mathbf{g}} \rangle_{\mathcal{V}} = \frac{1}{V}\int_{\mathcal{V}} \overline{\mathbf{g}} d\mathcal{V}. \tag{A.8}$$

In the above equation, V is the volume of the physical domain. Thus, Eq. (A.7) can be rewritten as:

$$\frac{\partial \overline{u}_i}{\partial \overline{t}} + \overline{S}_i = -\frac{1}{\rho_f}\langle \overline{g}_i \rangle_{\mathcal{V}} - \frac{1}{\rho_f}\frac{\partial \psi'}{\partial \overline{x}_i} + \nu_f \frac{\partial^2 \overline{u}_i}{\partial \overline{x}_j \partial \overline{x}_j} - A_{f,i}. \tag{A.9}$$

In the above equation, $\bar{\mathbf{g}}'$ is written as the gradient of a fluctuating pressure ψ'. In a similar fashion averaged fluid velocity can be estimated by averaging the fluid velocity fields over the fluid volume i.e.,

$$\left\langle \overline{u}_i^{(f)} \right\rangle = \frac{1}{V_f}\int_{\mathcal{V}_f} \overline{u}_i d\mathcal{V}_f. \tag{A.10}$$

where V_f is the volume of the region occupied by the fluid. The evolution equation for the phasic averaged fluid velocity can be obtained by integrating Eq. (A.9) over the fluid volume. The resulting equation is:

$$V_f \frac{d}{d\overline{t}}\left\langle \overline{u}_i^{(f)} \right\rangle = -\frac{1}{\rho_f}\langle \overline{g}_i \rangle_{\mathcal{V}} V_f + \frac{1}{\rho_f}\int_{\partial\mathcal{V}_s} \psi' n_i^{(s)} dA - \nu_f \int_{\partial\mathcal{V}_s} \frac{\partial \overline{u}_i}{\partial \overline{x}_j} n_j^{(s)} dA - A_{f,i} V_f. \tag{A.11}$$

In the above Equation $\partial\mathcal{V}_s$ denotes the solid surface bounding the fluid volume and $n_j^{(s)}$ denotes the component of normal vector pointing outward from the surface of the solid particles. Dividing the entire equation by the fluid volume V_f and rearranging the terms gives:

$$-\frac{1}{\rho_f}\langle \overline{g}_i \rangle_{\mathcal{V}} = \frac{d}{d\overline{t}}\left\langle \overline{u}_i^{(f)} \right\rangle + \frac{1}{(1-\phi)V}\left[-\frac{1}{\rho_f}\int_{\partial\mathcal{V}_s} \psi' n_i^{(s)} dA + \nu_f \int_{\partial\mathcal{V}_s} \frac{\partial \overline{u}_i}{\partial \overline{x}_j} n_j^{(s)} dA\right] + A_{f,i}. \tag{A.12}$$

Now, the equations of motion for the particles in the reference frame $\overline{E}$ will be derived. The velocity of the nth particle transforms as $\overline{\mathbf{V}}^{(n)}(t)=\mathbf{V}^{(n)}(t)-\mathrm{V}_f(t)$. Substituting the transformation rules in Eq. (A.3), the equation of motion for the nth particle is obtained as:

$$m\frac{d\overline{V}_i^{(n)}}{d\overline{t}} = -\langle \overline{g}_i \rangle_{\mathcal{V}} V^{(n)} + \rho_f\left[-\frac{1}{\rho_f}\int_{\partial v_s^{(n)}(t)} \psi' n_i^{(n)} dA + \nu_f \int_{\partial v_s^{(n)}(t)} \frac{\partial \overline{u}_i}{\partial \overline{x}_j} n_j^{(n)} dA\right] - m A_{f,i}. \tag{A.13}$$

The phasic mean solid velocity can be estimated as $u^{(s)} = (1/N_p)\sum_{n=1}^{N_p}\overline{V}^{(n)}$ where N_p is the total number of particles in the domain. The evolution equation for the mean solid velocity can be derived by summing Eq. (A.13) over all the particles. The resulting equation is:

$$\rho_p V_s \frac{d}{d\overline{t}}\left\langle \overline{u}_i^{(s)} \right\rangle = -\langle \overline{g}_i \rangle_{\mathcal{V}} V_s + \rho_f\left[-\frac{1}{\rho_f}\int_{\partial\mathcal{V}_s} \psi' n_i^{(s)} dA + \nu_f \int_{\partial\mathcal{V}_s} \frac{\partial \overline{u}_i}{\partial \overline{x}_j} n_j^{(s)} dA\right] - \rho_p V_s A_{f,i} \tag{A.14}$$

where ρ_p is the density of the particles and V_s is the total volume occupied by the solid phase. It should be noted that the surface integrals in Eq. (A.13) are taken over the surface of the nth particle and in Eq. (A.14), the surface integration is over all the solid surfaces. This is because,

$$\int_{\partial\mathcal{V}_s} = \sum_{n=1}^{N_p}\int_{\partial\mathcal{V}_s^{(n)}}.$$

Eq. (A.14) can be rewritten as

$$\frac{d}{d\overline{t}}\left\langle \overline{u}_i^{(s)} \right\rangle = -\frac{1}{\rho_p}\langle \overline{g}_i \rangle_{\mathcal{V}} + \frac{1}{\phi V}\frac{\rho_f}{\rho_p}\left[-\frac{1}{\rho_f}\int_{\partial\mathcal{V}_s} \psi' n_i^{(s)} dA + \nu_f \int_{\partial\mathcal{V}_s} \frac{\partial \overline{u}_i}{\partial \overline{x}_j} n_j^{(s)} dA\right] - A_{f,i}. \tag{A.15}$$

Rearranging the above equation, an equation for the mean pressure gradient can be obtained as

$$-\frac{1}{\rho_p}\langle \overline{g}_i\rangle_{\mathcal{V}} = \frac{d}{d\overline{t}}\left\langle \overline{u}_i^{(s)}\right\rangle - \frac{1}{\phi V}\frac{\rho_f}{\rho_p}\left[-\frac{1}{\rho_f}\int_{\partial\mathcal{V}_s}\psi' n_i^{(s)}dA + \nu_f\int_{\partial\mathcal{V}_s}\frac{\partial\,\overline{u}_i}{\partial\,\overline{x}_j}n_j^{(s)}dA\right] + A_{f,i}. \tag{A.16}$$

The total drag force on the particles denoted $\overline{\mathbf{F}}_D$ is given by

$$\overline{F}_{D,i} = \rho_f\left[-\frac{1}{\rho_f}\int_{\partial\mathcal{V}_s}\psi' n_i^{(s)}dA + \nu_f\int_{\partial\mathcal{V}_s}\frac{\partial\,\overline{u}_i}{\partial\,\overline{x}_j}n_j^{(s)}dA\right].$$

Using the above notation, Eqs. (A.12) and (A.16) can be simplified and summarized as follows:

$$-\frac{1}{\rho_f}\langle \overline{g}_i\rangle_{\mathcal{V}} = \frac{d}{d\,\overline{t}}\left\langle \overline{u}_i^{(f)}\right\rangle + \frac{1}{(1-\phi)V}\frac{\overline{F}_{D,i}}{\rho_f} + A_{f,i} \tag{A.17}$$

$$-\frac{1}{\rho_p}\langle \overline{g}_i\rangle_{\mathcal{V}} = \frac{d}{d\,\overline{t}}\left\langle \overline{u}_i^{(s)}\right\rangle - \frac{1}{\phi V}\frac{\overline{F}_{D,i}}{\rho_p} + A_{f,i}. \tag{A.18}$$

The above two systems of equations contain two unknowns namely the mean pressure gradient $\langle\overline{\mathbf{g}}\rangle_{\mathcal{V}}$ and the frame acceleration $A_{f,i}$. The frame acceleration can be eliminated from the above equations to give a general expression for the mean pressure gradient:

$$\left(\frac{1}{\rho_f}-\frac{1}{\rho_p}\right)\langle \overline{g}_i\rangle_{\mathcal{V}} = \frac{d}{d\,\overline{t}}\left\langle \overline{u}_i^{(s)}\right\rangle - \frac{d}{d\,\overline{t}}\left\langle \overline{u}_i^{(f)}\right\rangle - \frac{\overline{F}_{D,i}}{V}\left[\frac{1}{\phi\rho_p} + \frac{1}{(1-\phi)\rho_f}\right]. \tag{A.19}$$

The fixed particle simulations described in the paper are a special case where the particles are so massive that they do not move i.e., $\rho_p\to\infty$ and the rate of change of the mean solid velocity is zero. So taking the limit $\rho_p\to\infty$ in Eq. (A.19), we get

$$\frac{1}{\rho_f}\langle \overline{g}_i\rangle_{\mathcal{V}} = -\frac{d}{d\,\overline{t}}\left\langle \overline{u}_i^{(f)}\right\rangle - \frac{\overline{F}_{D,i}}{V}\frac{1}{(1-\phi)\rho_f} \tag{A.20}$$

which is the same as the one derived by [29].

The frame acceleration can be obtained from Eq. (A.18) as:

$$A_{f,i} = -\frac{1}{\rho_p}\langle \overline{g}_i\rangle_{\mathcal{V}} - \frac{d}{d\,\overline{t}}\left\langle \overline{u}_i^{(s)}\right\rangle + \frac{1}{\phi V}\frac{\overline{F}_{D,i}}{\rho_p} \tag{A.21}$$

It can be seen that the mean pressure gradient depends upon the rate of change of the fluid and solids velocity. Eqs. (A.19) and (A.21) can be discretized in time as follows:

$$\left(\frac{1}{\rho_f}-\frac{1}{\rho_p}\right)\langle \overline{g}_i\rangle_{\mathcal{V}}^{n+1} = -\frac{\left\langle \overline{u}_i^{(f)}\right\rangle^{n+1} - \left\langle \overline{u}_i^{(f)}\right\rangle^{n}}{\Delta\overline{t}} - \frac{\left\langle \overline{u}_i^{(s)}\right\rangle^{n+1} - \left\langle \overline{u}_i^{(s)}\right\rangle^{n}}{\Delta\overline{t}} \tag{A.22}$$

$$-\frac{\overline{F}_{D,i}^{n}}{\mathcal{V}}\left[\frac{1}{\phi\rho_p} + \frac{1}{(1-\phi)\rho_f}\right] \tag{A.23}$$

$$A_{f,i}^{n+1} = -\frac{1}{\rho_p}\langle \overline{g}_i\rangle_{\mathcal{V}}^{n+1} - \frac{\left\langle \overline{u}_i^{(s)}\right\rangle^{n+1} - \left\langle \overline{u}_i^{(s)}\right\rangle^{n}}{\Delta\,\overline{t}} + \frac{1}{\phi V}\frac{\overline{F}_{D,i}^{n}}{\rho_p}. \tag{A.24}$$

It is desired that the mean solids velocity be zero and that the mean fluid velocity be driven to a desired value $\langle\bar{\mathbf{u}}^{(f)}\rangle^{d}$ which is set by the Reynolds number. Substituting $\langle\bar{\mathbf{u}}^{(f)}\rangle^{n+1} = \langle\bar{\mathbf{u}}^{(f)}\rangle^{d}$ and $\langle\bar{\mathbf{u}}^{(s)}\rangle^{n+1} = 0$ in the above two equations and noting that the initial mean solids velocity is zero, the resulting numerical equations are:

$$\left(\frac{1}{\rho_f}-\frac{1}{\rho_p}\right)\langle \overline{g}_i\rangle_{\mathcal{V}}^{n+1} = -\frac{\left\langle \overline{u}_i^{(f)}\right\rangle^{d} - \left\langle \overline{u}_i^{(f)}\right\rangle^{n}}{\Delta\,\overline{t}} - \frac{\overline{F}_{D,i}^{n}}{V}\left[\frac{1}{\phi\rho_p} + \frac{1}{(1-\phi)\rho_f}\right] \tag{A.25}$$

and

$$A_{f,i}^{n+1} = -\frac{1}{\rho_p}\langle \overline{g}_i\rangle_{\mathcal{V}}^{n+1} + \frac{1}{\phi V}\frac{\overline{F}_{D,i}^{n}}{\rho_p}. \tag{A.26}$$

From the above analysis it can be seen that there are two free parameters in this problem namely the mean pressure gradient and the frame acceleration. The mean pressure gradient can be thought of as a means to set the desired average fluid velocity and the frame acceleration can be seen as a time varying body force which will be tuned at every instant to give the desired mean solids velocity.

Appendix B. Estimation of granular temperature from the DNS of freely evolving suspensions

Solving the equations of motion in an accelerating frame of reference using Eqs. (A.25) and (A.26) ensures that: (i) the mean solids velocity is zero and (ii) the mean fluid velocity is such that the desired Reynolds number (based on slip velocity) is attained. At every time instant, the mean solids velocity is estimated from the DNS as

$$\left\{\mathbf{u}^{(s)}\right\}(t) = \frac{1}{N_p}\sum_{n=1}^{N_p}\mathbf{V}^{(n)}. \tag{B.1}$$

The mean velocity of the solids is denoted $\{\mathbf{u}^{(s)}\}$ to point out the fact that it is only an estimate to the true mean which is denoted $\langle\mathbf{u}^{(s)}\rangle$. The fluctuating velocity of the nth particle $\mathbf{v}'^{(n)}$ is computed from DNS as

$$\mathbf{v}'^{(n)}(t) = \mathbf{V}^{(n)}(t) - \left\{\mathbf{u}^{(s)}\right\}(t). \tag{B.2}$$

At every time instant, the granular temperature is estimated using the formula

$$\{T\}(t) = \frac{1}{3N_p}\sum_{n=1}^{N_p}\left(\mathbf{v}'^{(n)}(t)\cdot\mathbf{v}'^{(n)}(t)\right). \tag{B.3}$$

It is important to note that in Eq. (B.2) particle velocity fluctuations are defined about the mean solids velocity which is estimated as a number average and not as a time average. Fig. 7(a) and (b) shows the evolution of mean solids velocity and mean fluid velocity in the moving frame and the frame velocity with respect to the laboratory frame for solid to fluid density ratios of 10 and 1000 respectively. The volume fraction and the mean flow Reynolds number for both suspensions are 0.2 and 20 respectively. From these figures we observe that the frame velocity (shown by ▽) varies linearly with time. Imbalance between the mean pressure gradient and the drag force acting on the particles causes the particles to accelerate in the laboratory frame. Acceleration of the moving frame accounts for this imbalance and ensures that the mean solids velocity is zero in the moving frame. We can clearly see from Fig. 7(a) and (b) that the mean solids velocity (shown by open circles) is indeed zero and that the mean fluid velocity (shown by □) is such that the desired slip velocity is attained. Thus, we can conclude that the granular temperature we estimate from DNS is indeed a measure of the strength of the particle velocity fluctuations.

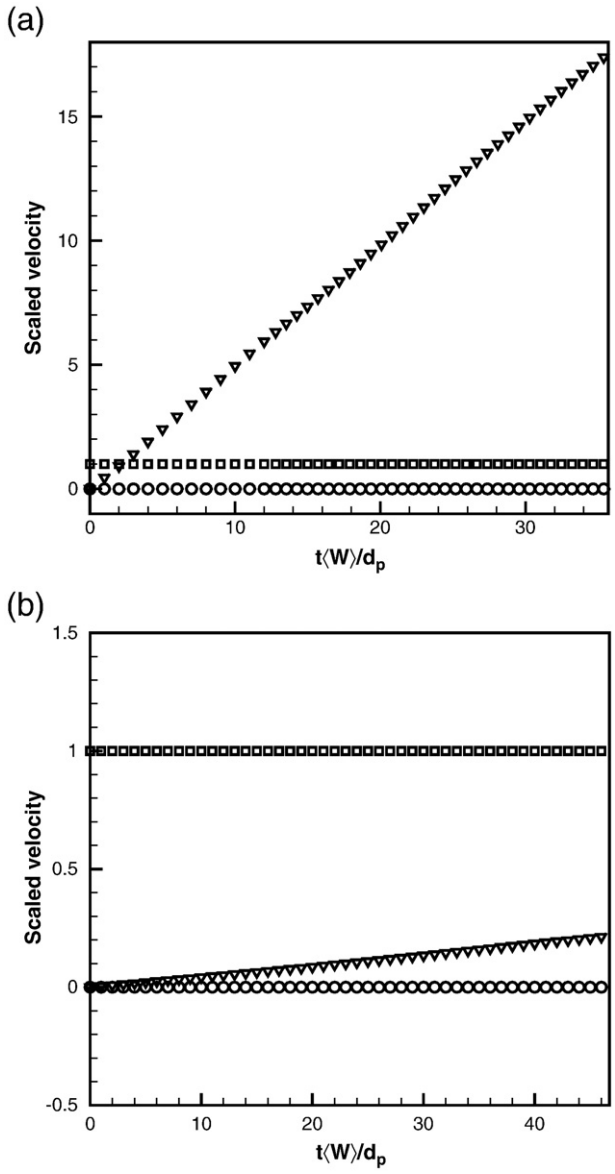

Fig. 7. Evolution of the mean solids velocity and mean fluid velocity in the moving frame and the frame velocity with respect to the laboratory frame obtained from the DNS of a freely evolving suspension of volume fraction 0.2, $Re_m = 20$. (a) Shows the results for a solid to fluid density ratio of 10 while (b) shows the results for a solid to fluid density ratio of 1000. In both figures, the mean solids velocity (open circles), the mean fluid velocity (□) and the frame velocity (▽) are scaled by the desired mean slip velocity.

References

[1] B. Halvorsen, C. Guenther, T.J. O'Brien, CFD Calculations for Scaling of a Bubbling Fluidized Bed, Proceedings of the AIChE Annual Meeting. AIChE, San Francisco, CA, 2003, pp. 16–21.

[2] T.B. Anderson, R. Jackson, A fluid mechanical description of fluidized beds: equations of motion, Ind. Eng. Chem. Fundam. 6 (4) (1967) 527–539.

[3] D.A. Drew, Mathematical modeling of two-phase flow, Annu. Rev. Fluid Mech. 15 (1983) 261–291.

[4] D.A. Drew, S.L. Passman, Theory of Multicomponent Fluids. Applied Mathematical Sciences, Springer, New York, 1998.

[5] C.M. Hrenya, J.L. Sinclair, Effects of particle-phase turbulence in gas–solid flows, AIChE J. 43 (4) (1997) 853–869.

[6] O. Simonin, Two-fluid Model Approach for Turbulent Reactive Two-phase Flows. Summer School on Numerical Modelling and Prediction of Dispersed Two-phase Flows, IMVU, Meserburg, Germany, 1995.

[7] E. Peirano, B. Leckner, Fundamentals of turbulent gas–solid flows applied to circulating fluidized bed combustion, Prog. Energy Combust. Sci. 24 (1998) 259–296.

[8] D.L. Koch, Kinetic theory for a monodisperse gas–solid suspension, Phys. Fluids 2 (10) (1990) 1711–1723.

[9] D.L. Koch, A.S. Sangani, Particle pressure and marginal stability limits for a homogeneous monodisperse gas-fluidized bed: kinetic theory and numerical simulations, J. Fluid Mech. 400 (1999) 229–263.

[10] J.J. Wylie, D.L. Koch, A.J. Ladd, Rheology of suspensions with high particle inertia and moderate fluid inertia, J. Fluid Mech. 480 (2003) 95–118.

[11] R. Glowinski, T.W. Pan, T.I. Hesla, D.D. Joseph, J. Périaux, A fictitious domain approach to the direct numerical simulation of incompressible viscous flow past moving rigid bodies: application to particulate flow, J. Comput. Phys. 169 (2) (2001) 363–426.

[12] M.G. Pai, S. Subramaniam, A comprehensive probability density function formalism for multiphase flows, J. Fluid Mech. 628 (2009) 181–228.

[13] R.W. Breault, C.P. Guenther, L.J. Shadle, 2008. Velocity fluctuation interpretation in the near wall region of a dense riser, Powder Technol. J. 182, 137–145.

[14] R.L. Liboff, Kinetic Theory: Classical, Quantum, and Relativistic Descriptions, 3rd EditionSpringer-Verlag, New York, 2003.

[15] S. Subramaniam, Statistical representation of a spray as a point process, Phys. Fluids 12 (10) (2000) 2413–2431.

[16] S. Subramaniam, Statistical modeling of sprays using the droplet distribution function, Phys. Fluids 13 (3) (2001) 624–642.

[17] V. Garzó, J.W. Dufty, C.M. Hrenya, Enskog theory for polydisperse granular mixtures, Phys. Rev. E Stat. Nonlinear Soft Matter Phys. 76 (3) (2007) 031303.

[18] F.A. Williams, Spray combustion and atomization, Phys. Fluids 1 (6) (1958) 541–545.

[19] M.H. Ernst, Nonlinear model-Boltzmann equations and exact solutions, Phys. Rep. 78 (1) (1981) 1–171.

[20] J.T. Jenkins, S.B. Savage, A theory for the rapid flow of identical, smooth, nearly elastic, spherical particles, J. Fluid Mech. 130 (1983) 187–201.

[21] C.K.K. Lun, S.B. Savage, D.J. Jeffrey, N. Chepurniy, Kinetic theories for granular flow — inelastic particles in Couette-flow and slightly inelastic particles in a general flowfield, J. Fluid Mech. 140 (1984) 223–256.

[22] N. Sela, I. Goldhirsch, Hydrodynamic equations for rapid flows of smooth inelastic spheres, J. Fluid Mech. 361 (1998) 41–74.

[23] V. Garzó, C.M. Hrenya, J.W. Dufty, Enskog theory for polydisperse granular mixtures. II. Sonine polynomial approximation, Phys. Rev. E Stat. Nonlinear Soft Matter Phys. 76 (3) (2007) 031304.

[24] C.Y. Wen, Y.H. Yu, Mechanics of fluidization, Chem. Eng. Prog. Symp. Ser. 62 (1966) 100–111.

[25] M. Syamlal, T. J. O'Brien, 1987. A generalized drag correlation for multiparticle systems. Tech. rep., Morgantown Energy Technology Center DOE Report.

[26] D. Gidaspow, Multiphase Flow and Fluidization, Academic Press, 1994.

[27] R.J. Hill, D.L. Koch, A.J.C. Ladd, The first effects of fluid inertia on flows in ordered and random arrays of spheres, J. Fluid Mech. 448 (2001) 213–241.

[28] R. Beetstra, M.A. van der Hoef, J.A.M. Kuipers, Drag force of intermediate Reynolds number flows past mono- and bidisperse arrays of spheres, AIChE J. 53 (2007) 489.

[29] R. Garg, S. Tenneti, J. Mohd-Yusof, S. Subramaniam, in press. Direct Numerical Simulation of Gas–Solids Flow Based on the Immersed Boundary Method. In: Pannala, S., Syamlal, M., O'Brien, T. J. (Eds.), Computational Gas–Solids Flows and Reacting Systems: Theory, Methods and Practice.

[30] A.S. Sangani, G. Mo, H.-K.W. Tsao, D.L. Koch, Simple shear flows of dense gas–solid suspensions at finite Stokes numbers, J. Fluid Mech. 313 (1996) 309–341.

[31] R. Garg, 2009. Modeling and simulation of two-phase flows. Ph.D. thesis, Iowa State University.

[32] A.A. Zick, G.M. Homsy, Stokes flow through periodic arrays of spheres, J. Fluid Mech. 115 (1982) 13–26.

[33] M.A. van der Hoef, R. Beetstra, J.A.M. Kuipers, Lattice-Boltzmann simulations of low-Reynolds-number flow past mono- and bidisperse arrays of sphere: results for the permeability and drag force, J. Fluid Mech. 528 (2005) 233–254.

[34] R.J. Hill, D.L. Koch, A.J.C. Ladd, Moderate-Reynolds-number flows in ordered and random arrays of spheres, J. Fluid Mech. 448 (2001) 243–278.

[35] J. Kim, P. Moin, Application of a fractional-step method to incompressible Navier–Stokes equations, J. Comput. Phys. 59 (1985) 308–323.

[36] X. Yin, D.L. Koch, Hindered settling velocity and microstructure in suspensions of spheres with moderate Reynolds number, Phys. Fluids 19 (2007) 093302.

[37] P.A. Cundall, O.D.L. Strack, A discrete numerical model for granular assemblies, Geotechnique 29 (1979) 47–65.

[38] R. Garg, J. Galvin, T. Li, S. Pannala, 2010a. Documentation of open-source MFIX–DEM software for gas–solids flows. Tech. rep., National Energy Technology Laboratory, Department of Energy. URL https://www.mfix.org.

[39] X. Yin, S. Sundaresan, Fluid–particle drag in low-Reynolds-number polydisperse gas–solid suspensions, AIChE J. 55 (2009) 1352–1368.

[40] S.B. Pope, Turbulent Flows, Cambridge University Press, Port Chester, NY, 2000 Ch. 2.